Supplement of Geosci. Model Dev., 16, 5685–5701, 2023
https://doi.org/10.5194/gmd-16-5685-2023-supplement

Geoscientific Model Development
Open Access
EGU

Supplement of

Dynamically weighted ensemble of geoscientific models via automated machine-learning-based classification

Hao Chen et al.

Correspondence to: Tiejun Wang (tiejun.wang@tju.edu.cn)

Table S1. An overview of Pedotransfer functions (PTFs) selected for modeling moisture retention characteristics in this study.

PTFs	Methods of PTFs	Source
Cosby0	Lookup table	Cosby et al. (1984)
Carsel & Parrish	Lookup table	Carsel and Parrish (1988)
Clapp & Hornberger	Lookup table	Clapp and Hornberger (1978)
Rosetta3-H1w	Lookup table	Zhang and Schaap (2017)
Cosby1	Regression equation	Cosby et al. (1984)
Cosby2	Regression equation	Cosby et al. (1984)
Rosetta3-H2*w*	Neural networks	Zhang and Schaap (2017)
Rawls & Brakensiek	Regression equation	Rawls and Brakensiek (1985)
Campbell & Shiozawa	Regression equation	Campbell and Shiozawa (1992)
Rosetta3-H3*w*	Neural networks	Zhang and Schaap (2017)
Wösten	Regression equation	Wösten et al. (1999)
Weynants	Regression equation	Weynants et al. (2009)
Vereecken	Regression equation	Vereecken et al. (1989)

* Abbreviated references, BC: Brooks and Corey (1964), BC-VG: BC parameters converted to VG parameters, CH: Clapp and Hornberger (1978), CMP: Campbell (1974), VG: van Genuchten (1980), VG*: modified van Genuchten (1980).

Table S2. Size of the sample labeled as individual PTFs.

PTFs	Sample size
Cosby0	7,360
Carsel & Parrish	9,051
Clapp & Hornberger	12,211
Rosetta3-H1w	7,476
Cosby1	6,884
Cosby2	6,882
Rosetta3-H2w	6,498
Rawls & Brakensiek	10,976
Campbell & Shiozawa	14,255
Rosetta3-H3w	7,563
Wösten	11,090
Weynants	9,634
Vereecken	8,719

Table S3. Computational demands and accuracy of ensemble predictions of designed machine learning classification models.

Classifier	Computational time (minutes)	R^2 (-)	RMSE (m^3/m^3)
Original_withSE	84.23	0.8629	0.0444
Balanced_withSE	84.37	0.8654	0.0440
Balanced_noSE	44.54	0.8480	0.0467
XGBoost_withSE	80.28	0.8600	0.0449
XGBoost_noSE	52.40	0.8480	0.0467
LGBM_noSE_30	12.07	0.8465	0.0472
LGBM_noSE_300	300.33	0.8505	0.0466

Specifically, we selected the case of assembling 13 PTFs and compared 7 different classifier configurations. These classifiers were evaluated based on their computational time and the accuracy of their ensemble predictions. Here, we utilized the H2O-AutoML platform and made use of its scenario (parameter) settings, particularly the include_algos or exclude_algos parameters (refer to the provided link: https://docs.h2o.ai/h2o/latest-stable/h2o-docs/parameters.html), to train the first 5 classifiers: 1) Original classifier (**Original_withSE**): This refers to the original classifier used in our study (consist of 6 different ML algorithms, 32 models including 2 stacked ensemble models). 2) Balanced classifier (**Balanced_withSE**): In this configuration, we enabled the balance_classes parameter in the original classifiers to handle the potential class imbalance issue. 3) Balanced classifier without the StackedEnsemble algorithm (**Balanced_noSE**): Here, we excluded the StackedEnsemble algorithm from the balanced classifier, meaning that no further ensemble of ML models was performed. 4) Original classifiers with only the XGBoost algorithm (**XGBoost_withSE**): Based on the original classifiers, we eliminated other algorithms except for the XGBoost and the StackedEnsemble algorithms. 5) XGBoost classifier without the StackedEnsemble algorithm (**XGBoost_noSE**): In this case, we considered only the XGBoost algorithm in the original classifier, without utilizing the StackedEnsemble algorithm. Throughout the H2O-AutoML training process, we still set the total number of models (max_models, https://docs.h2o.ai/h2o/latest-stable/h2o-docs/data-science/algo-params/max_models.html) to 30. For the 6th and 7th classifier, we opted to train the model in a Python environment using a combination of the state-of-the-art LightGBM algorithm (Ke et al., 2017) along with the efficient Optuna tool for accelerated hyperparameter optimization (Akiba et al., 2019). Note that a parameter called "n_trials", which represent the number of trials for each process in optimizing an objective function (https://optuna.readthedocs.io/en/stable/reference/generated/optuna.study.Study.html), were set to 30 and 300, respectively, thus, we obtained the other two classifiers, namely **LGBM_noSE_30** and **LGBM_noSE_300**. The configuration details can be found in the code we have shared and updated recently (https://doi.org/10.6084/m9.figshare.21547134.v3).

Table S4. List of 47 eddy covariance flux sites covering croplands from AmeriFlux (AM), AsiaFlux (AS), FLUXNET (FN), and European Flux Database Cluster (EF) networks. 'FN-AM' or 'FN-EF' indicates the site is available in both FN and AM or FN and EF and was retrieved from FN.

Site code	Cropland type	Country	Latitude	Longitude	Years	Network	MAP (mm)	MAT (°C)	Citation
BE-Lon	Dry	Belgium	50.5516	4.7461	2004-2014	FN-EF	800	10	Moureaux et al. (2006)
CH-Oe2	Dry	Switzer–land	47.2863	7.7343	2004-2014	FN-EF	1155	9.8	Moors et al. (2010)
CN-YCS	Dry	China	36.8290	116.5702	2003-2005	AS	528	13.1	http://asiaflux.net/?page_id=1178
DE-Geb	Dry	Germany	51.1001	10.9143	2001-2014	FN-EF	470	8.5	Anthoni et al. (2004)
DE-Kli	Dry	Germany	50.8929	13.5225	2004-2014	FN-EF	842	7.6	Brust et al. (2012)
DE-RuS	Dry	Germany	50.8659	6.4472	2011-2014	FN-EF	700	10	Eder et al. (2015)
DE-Seh	Dry	Germany	50.8706	6.4497	2007-2010	FN-EF	693	9.9	Korres et al. (2013)
DK-Ris	Dry	Denmark	55.5303	12.0972	2004-2008	EF	580	8	Kutsch et al. (2010)
ES-ES2	Paddy	Spain	39.2755	-0.3152	2004-2010	EF	550	18	Carvalhais et al. (2010)
FR-Aur	Dry	France	43.5496	1.1062	2005-2010	EF		12.9	B´eziat et al. (2009)
FR-Avi	Dry	France	43.9164	4.8792	2004-2006	EF	687	14	Kutsch et al. (2010)
FR-Gri	Dry	France	48.8442	1.9519	2004-2014	FN-EF	650	12	Loubet et al. (2011)
FR-Lam	Dry	France	43.4965	1.2379	2005-2010	EF		12.55	B´eziat et al. (2009)
IT-BCi	Dry	Italy	40.5238	14.9574	2004-2014	FN-EF	600	18	Ranucci et al. (2010)
IT-CA2	Dry	Italy	42.3772	12.0260	2011-2014	FN-EF	766	14	Sabbatini et al. (2016)

IT-Cas	Paddy	Italy	45.0628	8.6685	2006-2010	EF		11.9	Meijide et al. (2011)
JP-MSE	Paddy	Japan	36.0540	140.0269	2002-2006	AS			Muramatsu et al. (2017)
KR-CRK	Paddy	South Korea	38.2013	127.2507	2015	EF	1180.9	11.2	Yang et al. (2018)
US-ARM	Dry	USA	36.6058	–97.4888	2003-2012	FN-AM	843	14.76	Raz-Yaseef et al. (2015)
US-Bi1	Dry	USA	38.1022	-121.5042	2016-2018	AM	338	16	Hemes et al. (2019)
US-Bi2	Dry	USA	38.1090	-121.5350	2017-2018	AM	338	16	Hemes et al. (2019)
US-Bo1	Dry	USA	40.0062	-88.2904	2000-2008	AM	991.29	11.02	Bernacchi et al. (2005)
US-Bo2	Dry	USA	40.0090	-88.2900	2004-2006	AM	991.29	11.02	Bernacchi et al. (2005)
US-Br1	Dry	USA	41.9749	-93.6906	2005-2011	AM	842.33	8.95	Chu et al. (2018)
US-Br3	Dry	USA	41.9747	-93.6936	2005-2011	AM	846.6	8.9	Chu et al. (2018)
US-CRT	Dry	USA	41.6285	–83.3471	2011-2013	FN-AM	849	10.1	Chu et al. (2014)
US-Lin	Dry	USA	36.3600	-119.8400	2009-2010	FN-AM			Fares (2016)
US-Ne1	Dry	USA	41.1651	–96.4766	2001-2013	FN-AM	790	10.07	Verma et al. (2005)
US-Ne2	Dry	USA	41.1649	–96.4701	2001-2013	FN-AM	789	10.08	Suyker and Verma (2012)
US-Ne3	Dry	USA	41.1797	–96.4397	2001-2013	FN-AM	784	10.11	Suyker and Verma (2012)
US-Pon	Dry	USA	36.7667	-97.1333	2000	AM	866.34	14.94	Hanan et al. (2005)
US-RC1	Dry	USA	46.7837	-117.0777	2011-2016	AM	550	9	Lamb and Pressley (2016a)
US-RC2	Dry	USA	46.7776	-117.0807	2012-2016	AM	550	9	Lamb and Pressley (2016b)

US-RC3	Dry	USA	46.9910	-118.5980	2011-2016	AM	280	10	Lamb and Pressley (2016c)
US-RC4	Dry	USA	46.7580	-116.9490	2012-2016	AM	680	9	Lamb and Pressley (2016d)
US-Ro1	Dry	USA	44.7143	-93.0898	2004-2016	AM	879	6.4	Bavin et al. (2009)
US-Ro2	Dry	USA	44.7288	-93.0888	2015-2016	AM	879	6.4	Griffis et al. (2010)
US-Ro3	Dry	USA	44.7217	-93.0893	2004-2007	AM	879	6.4	Griffis et al. (2010)
US-Ro4	Dry	USA	44.6781	-93.0723	2014-2018	AM	879	6.4	Griffis et al. (2010)
US-Ro5	Dry	USA	44.6910	-93.0576	2017-2018	AM	879	6.4	Baker and Griffis (2016a)
US-Ro6	Dry	USA	44.6946	-93.0578	2017-2018	AM	879	6.4	Baker and Griffis (2016b)
US-SuM	Dry	USA	20.7981	-156.4540	2013-2014	AM	287	24.1	Anderson and Wang (2014)
US-SuS	Dry	USA	20.7847	-156.4039	2011-2014	AM	334	24.4	Anderson and Wang (2014)
US-SuW	Dry	USA	20.8246	-156.4913	2011-2013	AM	366	24.4	Anderson and Wang (2014)
US-Tw2	Dry	USA	38.1047	–121.6433	2012-2013	FN-AM	421	15.5	Knox et al. (2014)
US-Tw3	Dry	USA	38.1159	–121.6467	2013-2014	FN-AM	421	15.6	Baldocchi et al. (2015)
US-Twt	Paddy	USA	38.1087	–121.653	2009-2014	FN-AM	421	15.6	Hatala et al. (2012)

Table S5. A simplified summary of the six individual ET models selected in this study. An overview of the six ET models we used was presented in Appendix A and a summary of the key equations and their detailed descriptions of variables used in these models were presented in Table 2 and Table 3 in Bai et al. (2021), respectively.

Model name	Driving forces *	Reference
PT-JPL	VPD, T_a, R_n, NDVI, SAVI	Fisher et al. (2008); Vinukollu et al. (2011)
PT-DTsR	T_a, R_n, DTsR, NDVI	Yao et al. (2013)
STIC	T_a, VPD, u, R_n, T_R, NDVI	Mallick et al. (2014, 2015, 2016); Bhattarai et al. (2018)
SEBS	T_a, VPD, u, R_n, T_R, NDVI	Su (2002); Chen et al. (2013)
RS-WBPM	T_a, VPD, u, R_n, EVI, P_d	Bai et al. (2017)
EVI-PM	T_a, VPD, u, R_n, EVI	Yebra et al. (2013); Bai et al. (2017)

* Abbreviations, VPD: Vapor pressure deficit; T_a: Air temperature, R_n: Net radiation; NDVI: Normalized vegetation index; SAVI: Soil adjusted vegetation index; DTsR: Diurnal range of surface temperature retrieved from the MODIS thermal band; u: Wind speed; T_R: Land surface radiometric temperature; EVI: Enhanced vegetation index.

Table S6. Size of the sample labeled as individual ET models.

Model name	Sample size
PT-JPL	14,062
PT-DTsR	12,905
STIC	16,065
SEBS	12,903
RS-WBPM	16,869
EVI-PM	10,817

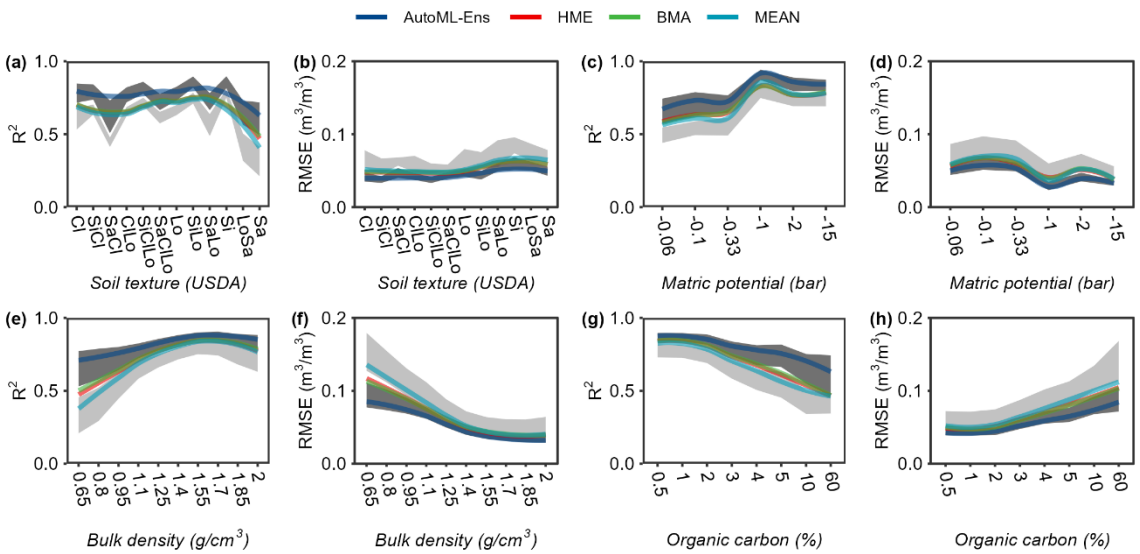

Figure S1. R^2 (**a**, **c**, **e**, **g**) and RMSE (**b**, **d**, **f**, **h**) when the moisture content estimates of different ensemble approaches were compared with observations (including all training and testing data) under various environmental conditions (6 variables, among which, the content of sand, silt, and clay was expressed together in terms of USDA soil texture classes) that were represented by predictors for AutoML-Ens. The light gray band denotes the uncertainties calculated as the mean±standard deviation of the R^2 (or RMSE) values of the 13 selected PTFs. The dark gray band denotes the uncertainties of the 6 individual ML algorithms.

S1. An overview of the MEAN, BMA, HME, and MLP methods.

1) The simple average (MEAN)

Previous studies revealed that a sample average of multi-model simulations may give better estimates than any individual model (e.g., Martre et al., 2015). In this study, we also evaluate the performance of an average of the soil water content (or LE) estimates ($\boldsymbol{y}$) from 13 PTFs (or six RS-based ET models) predictions ($\boldsymbol{p}$).

$$y_k = \frac{1}{N} \times \sum_{n=1}^{N} p_{k,n} \tag{S1}$$

where subscript k and n denote the index of a sample and model, respectively; N is the number of models.

2) Bayesian model averaging (BMA)

BMA (Raftery et al., 2005), which can be regarded as a direct application of Bayesian inference to the problem of ensemble estimation, is expected to be more effective than MEAN in assembling multiple models (Fragoso et al., 2018). Previous studies consider the problem of combining predictions from N models, $f_1, f_2, \cdots, f_N$ into one combined prediction. For each prediction, there is a probability density function (PDF) for the quantity one wished to predict y denoted by $g_l(y|f_l)$ for $l = 1, \cdots, N$. Afterwards, a combined density function using the weighted average is constructed as

$$g(y|f_1, \text{L} \ , f_N) = \sum_{l=1}^{N} w_1 \, \mathrm{g}_l(y|f_l) \tag{S2}$$

where w_l denotes the weight of the model f_l, in which $\sum_{l=1}^{N} w_l = 1$, and the weights are interpreted in an analogous fashion to the posterior probabilities of the model f_l. Assuming then each density as a normal, the weights are estimated using the expectation-maximization (EM) algorithm (Dempster et al., 1977).

Finally, the weights of the 13 PTFs (or six ET models) were obtained through the BMA approach, which are 0.02164, 0.00975, 0.05202, 0.01820, 0.05679, 0.03220, 0.04324, 0.07356, 0.01553, 0.24029, 0.24841, 0.16219, and 0.02618 for Cosby0, Carser & Parrish, Clapp & Hornberger, Rosetta3-H1*w*, Cosby1, Cosby2, Rosetta3-H2*w*, Rawls & Brakensiek, Campbell & Shiozawa, Rosetta3-H3*w*, Wösten, Weynants, and Vereecken PTF (or 0.217, 0.129, 0.199, 0.141,

0.150, and 0.164 for PT-JPL, PT-DTsR, STIC, SEBS, RS-WBPM, and EVI-PM model), respectively.

3) Hierarchical multi-model ensemble (HME)

The HME method was proposed by Zhang et al. (2020) for assembling the 13 selected PTFs. The weights of multi-PTF ensemble estimation are determined by minimizing the following:

$$\chi^2(\boldsymbol{W}) = \overline{\boldsymbol{\varepsilon}}\left(\overline{\boldsymbol{\varepsilon}}\right)^T$$
$$where \quad \overline{\boldsymbol{\varepsilon}} = \frac{1}{\sum_{j=1}^{N} w_j}\sum_{j=1}^{N} w_j\left(\theta' - \theta\right)^2 \tag{S3}$$

and $\boldsymbol{W}$ is a vector of weights, w_j, for corresponding PTF model P_j, where $j = 1, \cdots, N$, $0 \le w_j \le 1$, N is the number of PTF ensembles; θ and θ' are vectors of measured and predicted soil water content, the length of which is the size of calibration samples selected by the bootstrap (with 100 replicas) resampling process. Different algorithms were evaluated for minimization of equation (S3), and we found that a genetic algorithm (Scrucca, 2013) was the most effective method to optimize $\boldsymbol{W}$.

Finally, we got the weights of the 13 PTFs through the HME approach, which are 0.0330, 0.0106, 0.1437, 0.0250, 0.0257, 0.0264, 0.0414, 0.0325, 0.0858, 0.1704, 0.1980, 0.1854, and 0.0223 for Cosby0, Carser & Parrish, Clapp & Hornberger, Rosetta3-H1*w*, Cosby1, Cosby2, Rosetta3-H2*w*, Rawls & Brakensiek, Campbell & Shiozawa, Rosetta3-H3*w*, Wösten, Weynants, and Vereecken PTF, respectively.

4) The multi-layer perception neural network classifier (MLP)

MLP is a supplement of supervised feedforward neural network. It has been considered as learning a nonlinear functional mapping between a set of predictors $\boldsymbol{x}$ (or input layer) and a corresponding target variable y (or output layer), with an arbitrary number of hidden layers.

$$y = f(\boldsymbol{x}) + \varepsilon \tag{S4}$$

Each layer in the MLP contains neurons. With a multi-layer architecture, the neurons are trained to approximate any continuous multivariate function for either classification or regression. MLP intrinsically classifies an unknown sample based on the sample's computed probability of being each of the target classes, and the sample is assigned to the class with the highest probability. MLP, as a supervised learning algorithm, requires labeled training data to determine model parameters, such as the 'connection weight' between neurons, activation functions of hidden layers, and the numbers of hidden layers and neurons (Du and Swamy, 2014). In this study, the optimal

MLP turned out to have 2 hidden layers and 80 neurons in each layer with the activation of rectified linear unit function (relu).

References

Anderson, R. G., and D. Wang (2014), Energy budget closure observed in paired Eddy Covariance towers with increased and continuous daily turbulence, *Agricultural and Forest Meteorology*, *184*, 204-209. https://doi.org/10.1016/j.agrformet.2013.09.012

Anthoni, P. M., A. Knohl, C. Rebmann, A. Freibauer, M. Mund, W. Ziegler, O. Kolle, and E.-D. Schulze (2004), Forest and agricultural land-use-dependent CO2 exchange in Thuringia, Germany, *Global Change Biology*, *10*(12), 2005-2019. https://doi.org/10.1111/j.1365-2486.2004.00863.x

Bai, Y., J. Zhang, S. Zhang, U. A. Koju, F. Yao, and T. Igbawua (2017), Using precipitation, vertical root distribution, and satellite-retrieved vegetation information to parameterize water stress in a Penman-Monteith approach to evapotranspiration modeling under Mediterranean climate, *Journal of Advances in Modeling Earth Systems*, *9*(1), 168-192. https://doi.org/10.1002/2016MS000702

Baker, J., and T. Griffis (2018a), AmeriFlux AmeriFlux US-Ro5 Rosemount I18_South, edited, United States. https://doi.org/10.17190/AMF/1419508

Baker, J., and T. Griffis (2018b), AmeriFlux AmeriFlux US-Ro6 Rosemount I18_North, edited, United States. https://doi.org/10.17190/AMF/1419509

Baldocchi, D., C. Sturtevant, and F. Contributors (2015), Does day and night sampling reduce spurious correlation between canopy photosynthesis and ecosystem respiration?, *Agricultural and Forest Meteorology*, *207*, 117-126. https://doi.org/10.1016/j.agrformet.2015.03.010

Bavin, T. K., T. J. Griffis, J. M. Baker, and R. T. Venterea (2009), Impact of reduced tillage and cover cropping on the greenhouse gas budget of a maize/soybean rotation ecosystem, *Agriculture, Ecosystems & Environment*, *134*(3), 234-242. https://doi.org/10.1016/j.agee.2009.07.005

Bernacchi, C. J., S. E. Hollinger, and T. Meyers (2005), The conversion of the corn/soybean ecosystem to no-till agriculture may result in a carbon sink, *Global Change Biology*, *11*(11), 1867-1872. https://doi.org/10.1111/j.1365-2486.2005.01050.x

Béziat, P., E. Ceschia, and G. Dedieu (2009), Carbon balance of a three crop succession over two cropland sites in South West France, *Agricultural and Forest Meteorology*, *149*(10), 1628-1645. https://doi.org/10.1016/j.agrformet.2009.05.004

Bhattarai, N., K. Mallick, N. A. Brunsell, G. Sun, and M. Jain (2018), Regional evapotranspiration from an image-based implementation of the Surface Temperature Initiated Closure (STIC1.2) model and its validation across an aridity gradient in the conterminous US, *Hydrol. Earth Syst. Sci.*, *22*(4), 2311-2341. https://doi.org/10.5194/hess-22-2311-2018

Brooks, R., and Corey, A (1964). Hydraulic properties of porous media. *Hydrology Papers, Colorado State University*, *3*, 1-27.

Brust, K., M. Hehn, and C. Bernhofer (2012), Comparative analysis of matter and energy fluxes determined by Bowen Ratio and Eddy Covariance techniques at a crop site in eastern Germany, paper presented at EGU general assembly conference abstracts.

Campbell, G. S. (1974), A simple method for determining unsaturated conductivity from moisture retention data, *Soil Science*, *117*(6), 311-314. https://doi.org/10.1097/00010694-197406000-00001

Campbell, G. S., and Shiozawa S. (1992). Prediction of hydraulic properties of soils using particle-size distribution and bulk density data. In *Indirect methods for estimating the hydraulic properties of unsaturated soils* (pp. 717-328). Riverside: University of California.

Carvalhais, N., M. Reichstein, G. J. Collatz, M. D. Mahecha, M. Migliavacca, C. S. R. Neigh, E. Tomelleri, A. A. Benali, D. Papale, and J. Seixas (2010), Deciphering the components of regional net ecosystem fluxes following a bottom-up approach for the Iberian Peninsula, Biogeosciences, 7(11), 3707-3729. https://doi.org/10.5194/bg-7-3707-2010

Chen, X., Z. Su, Y. Ma, K. Yang, J. Wen, and Y. Zhang (2013), An Improvement of Roughness Height Parameterization of the Surface Energy Balance System (SEBS) over the Tibetan Plateau, *Journal of Applied Meteorology and Climatology*, *52*(3), 607-622. https://doi.org/10.1175/jamc-d-12-056.1

Chu, H., J. Chen, J. F. Gottgens, Z. Ouyang, R. John, K. Czajkowski, and R. Becker (2014), Net ecosystem methane and carbon dioxide exchanges in a Lake Erie coastal marsh and a nearby cropland, *Journal of Geophysical Research: Biogeosciences*, *119*(5), 722-740. https://doi.org/10.1002/2013JG002520

Chu, H., et al. (2018), Temporal Dynamics of Aerodynamic Canopy Height Derived From Eddy Covariance Momentum Flux Data Across North American Flux Networks, *Geophysical Research Letters*, *45*(17), 9275-9287. https://doi.org/10.1029/2018GL079306

Clapp, R. B., and G. M. Hornberger (1978), Empirical equations for some soil hydraulic properties, *Water Resources Research*, *14*(4), 601-604. https://doi.org/10.1029/WR014i004p00601

Cosby, B. J., G. M. Hornberger, R. B. Clapp, and T. R. Ginn (1984), A Statistical Exploration of the Relationships of Soil Moisture Characteristics to the Physical Properties of Soils, *Water Resources Research*, *20*(6), 682-690. https://doi.org/10.1029/WR020i006p00682

Dempster, A. P., N. M. Laird, and D. B. Rubin (1977), Maximum Likelihood from Incomplete Data Via the EM Algorithm, *Journal of the Royal Statistical Society: Series B (Methodological)*, *39*(1), 1-22. https://doi.org/10.1111/j.2517-6161.1977.tb01600.x

Du, K.-L., and M. N. S. Swamy (2014), Multilayer Perceptrons: Architecture and Error Backpropagation, in Neural Networks and Statistical Learning, edited, pp. 83-126, Springer London, London. https://doi.org/10.1007/978-1-4471-5571-3_4

Eder, F., M. Schmidt, T. Damian, K. Träumner, and M. Mauder (2015), Mesoscale Eddies Affect Near-Surface Turbulent Exchange: Evidence from Lidar and Tower Measurements, *Journal of Applied Meteorology and Climatology*, *54*(1), 189-206. https://doi.org/10.1175/jamc-d-14-0140.1

Fisher, J. B., K. P. Tu, and D. D. Baldocchi (2008), Global estimates of the land–atmosphere water flux based on monthly AVHRR and ISLSCP-II data, validated at 16 FLUXNET sites, *Remote Sensing of Environment*, *112*(3), 901-919. https://doi.org/10.1016/j.rse.2007.06.025

Griffis, T. J., J. M. Baker, S. D. Sargent, M. Erickson, J. Corcoran, M. Chen, and K. Billmark (2010), Influence of C4 vegetation on 13CO2 discrimination and isoforcing in the upper Midwest, United States, *Global Biogeochemical Cycles*, *24*(4). https://doi.org/10.1029/2009GB003768

Hanan, N. P., J. A. Berry, S. B. Verma, E. A. Walter-Shea, A. E. Suyker, G. G. Burba, and A. S. Denning (2005), Testing a model of CO2, water and energy exchange in Great Plains tallgrass prairie and wheat ecosystems, *Agricultural and Forest Meteorology*, *131*(3), 162-179. https://doi.org/10.1016/j.agrformet.2005.05.009

Hatala, J. A., M. Detto, and D. D. Baldocchi (2012), Gross ecosystem photosynthesis causes a diurnal pattern in methane emission from rice, *Geophysical Research Letters*, *39*(6). https://doi.org/10.1029/2012GL051303

Hemes, K. S., S. D. Chamberlain, E. Eichelmann, T. Anthony, A. Valach, K. Kasak, D. Szutu, J. Verfaillie, W. L. Silver, and D. D. Baldocchi (2019), Assessing the carbon and climate benefit of restoring degraded agricultural peat soils to managed wetlands, *Agricultural and Forest Meteorology*, *268*. https://doi.org/10.1016/j.agrformet.2019.01.017

Knox, S. H., C. Sturtevant, J. H. Matthes, L. Koteen, J. Verfaillie, and D. Baldocchi (2015), Agricultural peatland restoration: effects of land-use change on greenhouse gas (CO2 and CH4) fluxes in the Sacramento-San Joaquin Delta, *Global Change Biology*, *21*(2), 750-765. https://doi.org/10.1111/gcb.12745

Korres, W., T. G. Reichenau, and K. Schneider (2013), Patterns and scaling properties of surface soil moisture in an agricultural landscape: An ecohydrological modeling study, *Journal of Hydrology*, *498*, 89-102. https://doi.org/10.1016/j.jhydrol.2013.05.050

Kutsch, W. L., et al. (2010), The net biome production of full crop rotations in Europe, *Agriculture, Ecosystems & Environment*, *139*(3), 336-345. https://doi.org/10.1016/j.agee.2010.07.016

Lamb, B., and S. Pressley (2019a), AmeriFlux AmeriFlux US-RC1 Cook Agronomy Farm - No

Till, edited, United States. https://doi.org/10.17190/AMF/1498748

Lamb, B., and S. Pressley (2019b), AmeriFlux AmeriFlux US-RC2 Cook Agronomy Farm - Conventional Till, edited, United States. https://doi.org/10.17190/AMF/1498747

Lamb, B., and S. Pressley (2019c), AmeriFlux AmeriFlux US-RC3 WSU Lind Dryland Research Station, edited, United States. https://doi.org/10.17190/AMF/1498749

Lamb, B., and S. Pressley (2019d), AmeriFlux AmeriFlux US-RC4 Moscow Mountain on-farm site, edited, United States. https://doi.org/10.17190/AMF/1498750

Loubet, B., et al. (2011), Carbon, nitrogen and Greenhouse gases budgets over a four years crop rotation in northern France, *Plant and Soil*, *343*(1/2), 109-137. https://doi.org/10.1007/s11104-011-0751-9

Mallick, K., et al. (2015), Reintroducing radiometric surface temperature into the Penman-Monteith formulation, *Water Resources Research*, *51*(8), 6214-6243. https://doi.org/10.1002/2014WR016106

Mallick, K., et al. (2014), A Surface Temperature Initiated Closure (STIC) for surface energy balance fluxes, *Remote Sensing of Environment*, *141*, 243-261. https://doi.org/10.1016/j.rse.2013.10.022

Mallick, K., et al. (2016), Canopy-scale biophysical controls of transpiration and evaporation in the Amazon Basin, *Hydrol. Earth Syst. Sci.*, *20*(10), 4237-4264. https://doi.org/10.5194/hess-20-4237-2016

Martre, P., et al. (2015), Multimodel ensembles of wheat growth: many models are better than one, *Global Change Biology*, *21*(2), 911-925. https://doi.org/10.1111/gcb.12768

Meijide, A., G. Manca, I. Goded, V. Magliulo, P. di Tommasi, G. Seufert, and A. Cescatti (2011), Seasonal trends and environmental controls of methane emissions in a rice paddy field in Northern Italy, *Biogeosciences*, *8*(12), 3809-3821. https://doi.org/10.5194/bg-8-3809-2011

Moors, E. J., et al. (2010), Variability in carbon exchange of European croplands, *Agriculture, Ecosystems & Environment*, *139*(3), 325-335. https://doi.org/10.1016/j.agee.2010.04.013

Moureaux, C., A. Debacq, B. Bodson, B. Heinesch, and M. Aubinet (2006), Annual net ecosystem carbon exchange by a sugar beet crop, *Agricultural and Forest Meteorology*, *139*(1), 25-39. https://doi.org/10.1016/j.agrformet.2006.05.009

Muramatsu, K., K. Ono, N. Soyama, T. Juthasinee, A. Miyata, and M. Mano (2017), Determination of rice paddy parameters in the global gross primary production capacity estimation algorithm using 6 years of JP-MSE flux observation data, *Journal of Agricultural Meteorology*, *73*(3), 119-132. https://doi.org/10.2480/agrmet.D-16-00017

Raftery, A. E., T. Gneiting, F. Balabdaoui, and M. Polakowski (2005), Using Bayesian model

averaging to calibrate forecast ensembles, *Monthly Weather Review*, *133*(5), 1155-1174. https://doi.org/10.1175/MWR2906.1

Ranucci, S., T. Bertolini, L. Vitale, P. Tommasi, L. Ottaiano, M. Oliva, U. Amato, A. Fierro, and V. Magliulo (2011), The influence of management and environmental variables on soil N 2 O emissions in a crop system in Southern Italy, *Plant and Soil*, *343*. https://doi.org/10.1007/s11104-010-0674-x

Rawls, W. J., and D. L. Brakensiek (1985), Prediction of soil water properties for hydrologic modeling. In *Watershed management in the eighties* (pp. 293-299). New York, NY: Proceedings of the American Society of Cicil Engineers.

Raz-Yaseef, N., D. P. Billesbach, M. L. Fischer, S. C. Biraud, S. A. Gunter, J. A. Bradford, and M. S. Torn (2015), Vulnerability of crops and native grasses to summer drying in the U.S. Southern Great Plains, *Agriculture, Ecosystems & Environment*, *213*, 209-218. https://doi.org/10.1016/j.agee.2015.07.021

Sabbatini, S., N. Arriga, B. Gioli, D. Papale, A. Boschi, and M. Tomassucci (2016), FLUXNET2015 IT-CA2 Castel d'Asso2, edited, Italy. https://doi.org/10.18140/FLX/1440231

Scrucca, L. (2013), GA: A Package for Genetic Algorithms in R, Journal of Statistical Software, 53(4), 1 - 37. https://doi.org/10.18637/jss.v053.i04

Su, Z. (2002), The Surface Energy Balance System (SEBS) for estimation of turbulent heat fluxes, *Hydrol. Earth Syst. Sci.*, *6*(1), 85-100. https://doi.org/10.5194/hess-6-85-2002

Suyker, A. E., and S. B. Verma (2012), Gross primary production and ecosystem respiration of irrigated and rainfed maize–soybean cropping systems over 8 years, *Agricultural and Forest Meteorology*, *165*, 12-24. https://doi.org/10.1016/j.agrformet.2012.05.021

van Genuchten, M. T. (1980), A Closed-form Equation for Predicting the Hydraulic Conductivity of Unsaturated Soils, *Soil Science Society of America Journal*, *44*(5), 892-898. https://doi.org/10.2136/sssaj1980.03615995004400050002x

Vereecken, H., J. Maes, J. Feyen, and P. Darius (1989), Estimating the soil moisture retention characteristic from texture, bulk density, and carbon content, *Soil Science*, *148*(6), 389-403.

Verma, S. B., et al. (2005), Annual carbon dioxide exchange in irrigated and rainfed maize-based agroecosystems, *Agricultural and Forest Meteorology*, *131*(1), 77-96. https://doi.org/10.1016/j.agrformet.2005.05.003

Vinukollu, R. K., E. F. Wood, C. R. Ferguson, and J. B. Fisher (2011), Global estimates of evapotranspiration for climate studies using multi-sensor remote sensing data: Evaluation of three process-based approaches, *Remote Sensing of Environment*, *115*(3), 801-823. https://doi.org/10.1016/j.rse.2010.11.006

Weihermüller, L., M. Herbst, M. Javaux, and M. Weynants (2017), Erratum to "Revisiting Vereecken Pedotransfer Functions: Introducing a Closed-Form Hydraulic Model", *Vadose Zone Journal*, *16*(1), vzj2008.0062er. https://doi.org/10.2136/vzj2008.0062er

Weynants, M., H. Vereecken, and M. Javaux (2009), Revisiting Vereecken Pedotransfer Functions: Introducing a Closed-Form Hydraulic Model, *Vadose Zone Journal*, *8*(1), 86-95. https://doi.org/10.2136/vzj2008.0062

Yang, K., et al. (2018), Sun-induced chlorophyll fluorescence is more strongly related to absorbed light than to photosynthesis at half-hourly resolution in a rice paddy, *Remote Sensing of Environment*, *216*, 658-673. https://doi.org/10.1016/j.rse.2018.07.008

Yao, Y., et al. (2013), MODIS-driven estimation of terrestrial latent heat flux in China based on a modified Priestley–Taylor algorithm, *Agricultural and Forest Meteorology*, *171-172*, 187-202. https://doi.org/10.1016/j.agrformet.2012.11.016

Yebra, M., A. Van Dijk, R. Leuning, A. Huete, and J. P. Guerschman (2013), Evaluation of optical remote sensing to estimate actual evapotranspiration and canopy conductance, *Remote Sensing of Environment*, *129*, 250-261. https://doi.org/10.1016/j.rse.2012.11.004

Zhang, Y., and M. G. Schaap (2017), Weighted recalibration of the Rosetta pedotransfer model with improved estimates of hydraulic parameter distributions and summary statistics (Rosetta3), *Journal of Hydrology*, *547*, 39-53. https://doi.org/10.1016/j.jhydrol.2017.01.004